Korean J. Chem. Eng., **29**(2), 235-242 (2012)
DOI: 10.1007/s11814-011-0153-y

Oxygen permeation performance of $Ba_{0.5}Sr_{0.5}Co_{0.8}Fe_{0.2}O_{3-\delta}$ membrane after surface modification

Jung Hoon Park*,†, Edoardo Magnone*, Jong Pyo Kim, and Soo Hyun Choi***

*Greenhouse Gas Research Center, Korea Institute of Energy Research, 71-2, Jang-dong, Yuseong-gu, Daejeon 305-343, Korea
**Chemical Engineering, Chungnam National University, 220, Gung-dong, Yuseong-gu, Daejeon 305-764, Korea
(*Received 16 February 2011 • accepted 8 June 2011*)

Abstract−The effect of minor surface modification on the performance of $Ba_{0.5}Sr_{0.5}Co_{0.8}Fe_{0.2}O_{3-\delta}$ membrane was evaluated in the temperature region from 700 to 850 °C. Oxygen permeation experiments were conducted according to membrane thickness (1.0 mm and 1.6 mm) and oxygen partial pressure (0.21, 0.42, and 0.63 atm) in the absence and in the presence of carbon dioxide (300 and 500 ppm). The oxygen permeation flux of $Ba_{0.5}Sr_{0.5}Co_{0.8}Fe_{0.2}O_{3-\delta}$ membrane increased with increasing temperature and decreasing membrane thickness. The oxygen permeation flux through the membrane of 1.0 mm thickness with $Ba_{0.5}Sr_{0.5}Co_{0.8}Fe_{0.2}O_{3-\delta}$-modified surface was *ca.* 1.23 ml/cm^2·min at 850 °C under air feeding condition. It was found that the $Ba_{0.5}Sr_{0.5}Co_{0.8}Fe_{0.2}O_{3-\delta}$-modified $Ba_{0.5}Sr_{0.5}Co_{0.8}Fe_{0.2}O_{3-\delta}$ membrane has better oxygen permeation flux than the pristine $Ba_{0.5}Sr_{0.5}Co_{0.8}Fe_{0.2}O_{3-\delta}$ membrane. In summary, it has been demonstrated that the surface morphology is an important factor in determining the oxygen permeation fluxes through $Ba_{0.5}Sr_{0.5}Co_{0.8}Fe_{0.2}O_{3-\delta}$ membrane under mixed-control conditions.

Key words: Ion Transport Membrane, $Ba_{0.5}Sr_{0.5}Co_{0.8}Fe_{0.2}O_{3-\delta}$ (BSCF), Surface Modifications, Oxygen Permeation, Membrane Stability

INTRODUCTION

Mixed ionic-electronic conducting (MIEC) ceramic-based oxides are an exciting class of materials with many potential applications [1,2]. $Ba_{0.5}Sr_{0.5}Co_{0.8}Fe_{02}O_{3-\delta}$ (BSCF) is an important MIEC material of modern technology which has been widely used in different areas of research, for example, in novel alkaline earth metal based perovskite-type membrane for efficient oxygen separation and energy appliances that generate electricity and heat from various fuels [3-8].

It is well known that the oxygen permeation flux properties of the BSCF perovskite-type oxides could be modified by 1) tuning the composition of the MIEC material [8,9], 2) improving the surface exchange kinetics on the membrane surface through a surface modification when the oxygen permeation is limited by oxygen surface-exchange kinetics [10] and 3) reducing membrane thickness when the oxygen permeation is mostly limited by bulk diffusion across the BSCF membrane [11]. The oxygen permeation flux can be increased by reducing the thickness (L) of the MIEC membrane but in the case that L is smaller than the critical thickness (L_c), the oxygen permeability is controlled mainly by the oxygen surface exchange and this reaction becomes the rate determining step of the overall oxygen permeation process [12]. On the other hand, according to the Wagner equation, if the oxygen transfer is limited by its bulk diffusion ($L>L_c$), the oxygen permeation flux is inversely proportional to the thickness of the MIEC membrane. For the same microstructure, this regime is valid if one assumes that bulk properties of MIEC materials dominate the overall transport of oxygen through the MIEC membrane. As a result, for MIEC membrane with a thickness $L>L_c$ the oxygen permeation process is bulk diffusion limited with a marginal contribution of surface gas-exchange processes. In this connection, it has been noted by Bouwmeester et al. that the L_c values increase with increasing temperature [12] where, at the same time, the different values of L_c can vary depending on the composition, morphology and microstructure [13-16].

At the risk of oversimplification, Fig. 1(a)-(c) shows a schematic representation about the effect of a membrane thickness on oxygen permeation mechanism; bulk diffusion limitation (Fig. 1(a)), surface-limited kinetics control (Fig. 1(c)) and mixed control region (Fig. 1(b)). As expected, for an intermediate thickness regime ($L\cong L_c$), oxygen permeation flux is controlled by both elementary bulk diffusion and surface exchange kinetics. With decreasing BSCF membrane thickness, contribution of bulk diffusion resistance decreases, while contributions of surface reaction resistances increase. Recently, it was found that the surface reaction resistance of the permeate side is 2-6 times larger than feed-side resistance and the resistance contribution of bulk diffusion for overall resistance is more than 98% with a membrane thickness of 4-5 mm [17].

There is, in addition, a small discrepancy but not negligible in the different experimental results reported in the literature for the thickness values of L_c. Muydinov et al. [11] and Hong et al. [18] concluded that the oxygen permeability is controlled mainly by the oxygen diffusion in the bulk when the thickness is larger than 1.0-1.1 and 0.55 mm thick in the BSCF and BSCF-coated BSCF membranes, respectively. Yu et al. suggested that the oxygen permeability is limited by the diffusion oxygen ions in the thick BSCF and thus, in going to BSCF membrane below 1.0 mm thickness, oxygen transfer is limited by a process other than diffusion across the BSCF membrane [11]. Additionally, theoretical investigation indicated that bulk diffusion and surface oxygen exchange reactions

†To whom correspondence should be addressed.
E-mail: pjhoon@kier.re.kr

jointly controlled the overall oxygen permeation flux kinetics with a BSCF membrane thickness between 0.75 and 1.1 mm [19] and at thickness greater than 1.85 mm the oxygen permeability through BSCF membrane is limited by bulk diffusion without any apparent contribution of the surface exchange resistance at temperature of 700-900 °C [20].

In conclusion, as discussed above, it is well established that the oxygen permeation flux through the BSCF membrane is determined by the balance of the bulk diffusion to the surface exchange rates because mixed-control conditions is basically a combination of both resistances. The oxygen permeation through BSCF membranes with a thickness of about 1.0 mm is found to fall in the transition region ($L \cong L_c$) where both bulk processes and surface reaction contribute to the limitation of oxygen permeation flux. The present work will focus on the oxygen permeation under conditions of mixed control between bulk diffusion and oxygen surface-exchange reactions in more detail. In this connection oxygen permeation experiments were conduced according to BSCF membrane in the range of thickness from 1.6 to 1.0 mm, surface modification of BSCF dense membrane, oxygen partial pressure with carbon dioxide and temperature. This work is devoted to investigate influence of surface modification of BSCF membrane on oxygen permeation flux. The detailed morphology analysis of surface modifications was made with scanning electron microscope (SEM).

MATERIAL AND METHOD

All BSCF powder has been synthesized using polymerized complex method. The method of preparation was described in detail elsewhere [21]. The as-synthesized powders were compressed into disks of 20 mm in diameter and 1.0-2.0 mm of thickness in a stainless steel mold under a hydraulic load by unilateral press (model 25601 series, Specac Limited, U.K.). The green disk was sintered at 1,100 °C for 2 hr. The sintered BSCF dense disk was polished to smooth the surface and to control the thickness with 600 grit SiC. BSCF films were screen-printed on polished BSCF dense membrane disks using the same powders prepared from the polymerized complex method followed by high-temperature annealing (950 °C; 2 h). BSCF slurry with ethanol was made by hand mixing using an agate mortar with a pestle. The coating surfaces before and after lightly brushing off to remove excess powder with another paintbrush are schematically displayed in Fig. 1(d) and Fig. 1(e), respectively.

The crystal structures were characterized by x-ray diffraction (CuK_α =1.5405 Å) in the Bragg angle range from 20 to 70°. X-ray powder diffraction measurements (Rigaku Co Model D/Max 2200-Ultima-plus, Japan) were performed with a scan step of 0.05° at room temperature. The morphology of membranes was analyzed using a scanning electron microscope (SEM, Model 1530, LEO Co. Germany).

The experimental equipment for oxygen permeation test at high temperature was described in our previous work [21]. The leakage through membrane during oxygen permeation test was measured for all runs at each temperature and the oxygen permeation fluxes were corrected on the basis of the measured leakage using Eq (1):

$$JO_2\ [ml/cm^2 \cdot min\ (STP)] = \{F_{total}\ [ml/min]\ yO_2\ [v\%] - \text{leakage correction}\}/A\ [cm^2] \quad (1)$$

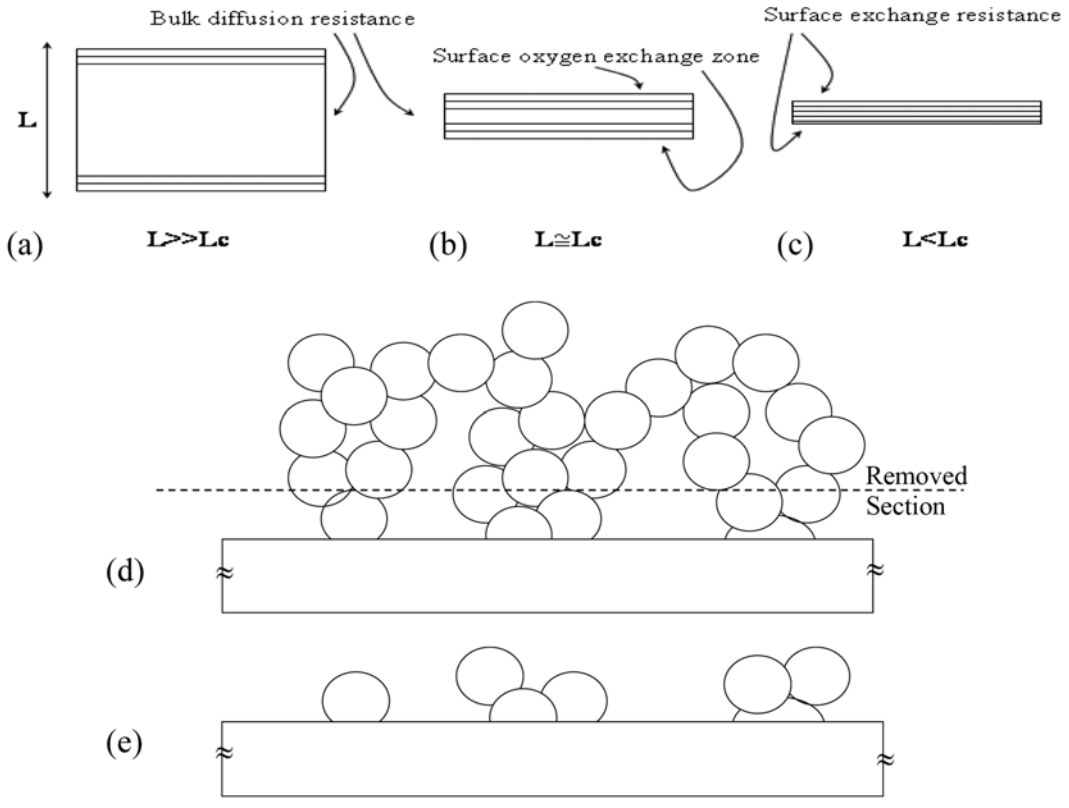

Fig. 1. Schematic representation of (a)-(c) surface exchange rate and the oxygen bulk diffusion resistance, (d) BSCF films deposited on BSCF dense membrane and (e) BSCF-modified BSCF membrane.

where F_{total} is the total flow rate of the permeation stream in which the oxygen concentration is yO_2. A is the effective membrane surface area, and leakage correction means the calculating oxygen permeation flux from leakage. Permeation study was performed within the temperature range of 700-850 °C at the steady state condition. The temperature of the permeation cell test was increased step-by-step from 700 to 850 °C to the desired temperature, using an increment of 50 °C, at a rate of 1.0 °C/min. The details of the experimental procedure have been previously described in Ref. [21]. The feed side of the membrane was flushed with pure air (99.999%) in the absence and in the presence of carbon dioxide (300 and 500 ppm). The feeding and sweeping flow rates were kept at 20 ml/min, respectively. Helium (99.999%) was used as a reference gas. The oxygen content in the permeate stream was measured with a gas chromatograph (GC-TCD, Acme 6000, YoungLin, Korea).

RESULTS AND DISCUSSION

To make sure that the materials were single phase perovskite-type with the cubic unit cell without any impurities, XRD was applied for crystal structure analysis of BSCF powders. The XRD pattern of the BSCF membrane heated at 1,100 °C for 2 h in synthetic air is shown in Fig. 2. The positions of the allowed hkl reflections are characteristic of the cubic crystal system [22]. Fig. 2 shows well-defined (*110*) peak at around 32° in the 2θ scale. No extra peaks were observed in the XRD patterns of BSCF surface membrane and then there was no evidence for impurities. Additionally, the microstructures of BSCF membrane sintered at 1,100 °C are given in Fig. 2. As one can see from inset of Fig. 2, it is observed that the average grain size is of the order of 10-50 μm. The BSCF membrane surface looks very dense with no porosity and, in summary, it can be concluded that the surface of BSCF membranes was dense and smooth.

Scanning electron microscopy has also been conducted to investigate the microstructural characteristics of the BSCF-modified BSCF membrane before and after partially removing the BSCF powder coated on the BSCF dense membrane, as schematically reported in Fig. 1(d) and Fig. 1(e), respectively. SEM micrographs of BSCF-modified BSCF membrane at different magnifications are presented in Fig. 3. On SEM micrographs, BSCF film is visible as homogeneously dispersed BSCF powders on the surface of the dense membrane. To further investigate the structure of this sample, we studied the morphology of BSCF powder by SEM at two different magnifications as shown in Fig. 3(b), (c). An electron micrograph of the BSCF surface, Fig. 3(b), clearly demonstrated the porous nature of the BSCF film. Moreover, it is observed that the BSCF film over the whole BSCF membrane is composed of well-dispersed non-spherical-type particles ranging in size from about 5 μm to 10 μm (Fig. 3(c)).

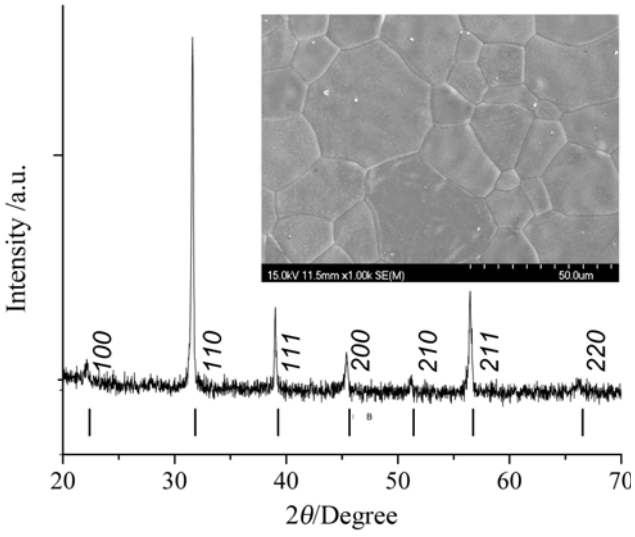

Fig. 2. The XRD pattern of fresh BSCF membrane before surface modification. Inset: SEM image of fresh BSCF membrane before surface modification.

The spatial distribution of the BSCF powder clusters was successively observed by SEM. Fig. 3(d)-(f) shows the surface morphology of BSCF-coated BSCF membrane after lightly brushing with paintbrush. As a reference, Fig. 1(e) shows the schematic representation of BSCF-modified BSCF membrane used in this study. Similarly, small granular ceramic particles existed on the top of dense BSCF membrane (Fig. 3(d)) after brushing. This set of small granular ceramic particles is randomly distributed on the surface of membrane. It is clear that the shape of BSCF-modified BSCF membrane is less regular and the surface is not smoother compared with that of the pristine BSCF surface membrane, *cf.* inset of Fig. 2. The diameters of the granular BSCF clusters were estimated to be about ≤20 μm (Fig. 3(d)).

Fig. 4 shows oxygen permeation flux of BSCF-modified BSCF membrane with different thickness in the range of mixed-control conditions with air (P_h=0.21 atm) and helium ($P_l=10^{-5}$ atm) in feed side and permeation side of membrane, respectively. According to Arrhenius' law, the oxygen permeation flux of the membranes increased with temperature in both cases. As BSCF membrane thickness decreased from 1.6 mm to 1.0 mm, the oxygen permeation flux increased about 100% from ~0.6 ml/cm^2·min at 850 °C. A maximum oxygen permeation flux was about 1.23 ml/cm^2·min at 850 °C with a 1 mm thick BSCF-modified BSCF membrane. The present results are in good agreement with the trend of the oxygen permeation flux for the BSCF solid solution systems reported in the literature [23,24]. Moreover, it is generally believed that if only one mechanism dominates during the oxygen permeation in the examined condition, the lines in the Arrhenius plot would be linear and parallel. Consequently, if different mechanisms occur during the oxygen permeation in different-controlled regimes, they would show unparallel lines. It is also assumed that straight lines diverge in different degrees from one to another regime, which imply that our mixed-control conditions model for BSCF-modified BSCF membrane is fundamentally valid to describe the partial overlapping between the different bulk diffusion and surface exchange contributions. In fact, as observed from Fig. 4, it can be note that the inclination of the oxygen permeation flux increased with the increase of L from 1 to 1.6 mm thickness, whereas the apparent oxygen exchange resistance contribution of surface reaction is very small ($L>L_c$). In this last case, if the oxygen exchange resistance on the surface of BSCF membrane is negligible, as also indicated in the introduction section of this paper, it indicates that the oxygen permeation flux of BSCF-modified BSCF membrane is controlled by bulk diffusion with Wagner equation (Eq. (2)):

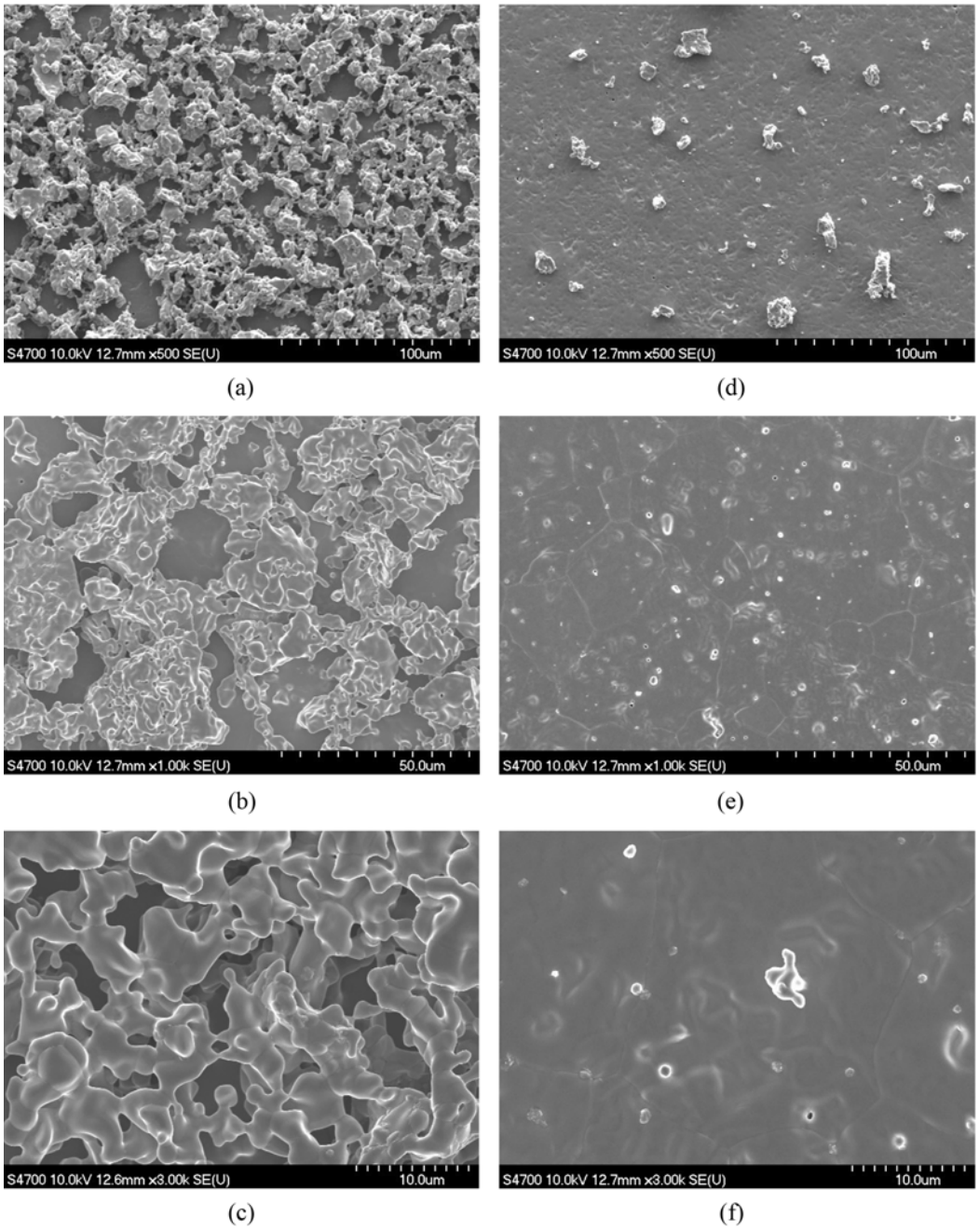

Fig. 3. SEM images of BSCF membrane surfaces after BSCF surface treatment through screen printing ((a), (b), (c)) and after lightly brushing off to remove excess powder ((d), (e), (f)).

$$Jo_2 = -\frac{RT}{4^2F^2L}\left(\frac{\sigma_i\sigma_e}{\sigma_i+\sigma_e}\right)\ln\left(\frac{P_1}{P_2}\right) \quad (2)$$

where R, T, F and L are the gas constant, Kelvin temperature, Faraday's constant and the BSCF membrane thickness, respectively; σ_i and σ_e are the ionic and electronic conductivities, respectively; and P_1 and P_2 are the high and low oxygen partial pressures on the two sides of the BSCF membrane, respectively. In other words, under mixed-control condition, morphology effect such as very small modification of membrane surface also play a role and cannot be ignored.

The oxygen permeability was measured as a function of temperature (850, 800, 750 and 700 °C) for a stepwise exposure to different oxygen partial pressure (0.21, 0.42 and 0.63 atm). Fig. 5 shows the dependence of oxygen permeation flux on the temperature and oxygen partial pressure for (a) BSCF membrane and (b) BSCF-modified BSCF membrane with 1 mm thickness under mixed-control conditions. Based on oxygen permeation flux measurements, it was found out that the oxygen permeation flux increases significantly with temperature under higher oxygen partial pressure conditions in both cases, and it reached to ~3.0 ml/cm^2·min at 850 °C exposed to oxygen partial pressure of 0.63 atm (Fig. 5(b)) in the case of BSCF-modified BSCF membrane. In addition, the highest oxygen permeation flux obtained for the pristine BSCF membrane was of ~1.4 ml/cm^2·min under high oxygen partial pressure (Po_2=0.63 atm) at

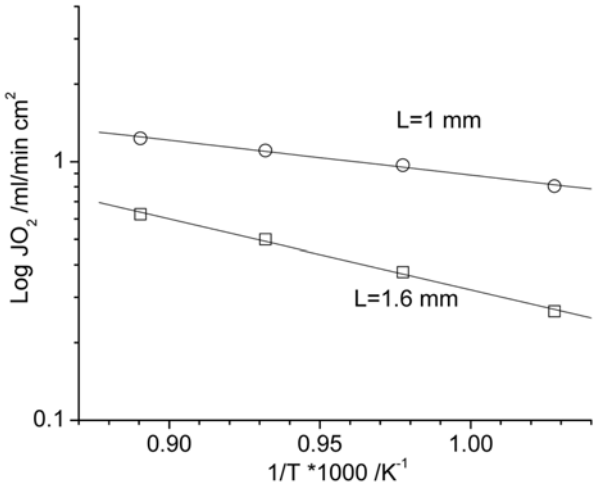

Fig. 4. Arrhenius plot of ln JO_2 of BSCF-modified BSCF membrane as a function of 1/T for two different membrane thicknesses (L=1.0 and 1.6 mm) at oxygen partial pressure of 0.21 atm. The data cover the temperature range from 850 to 750 °C.

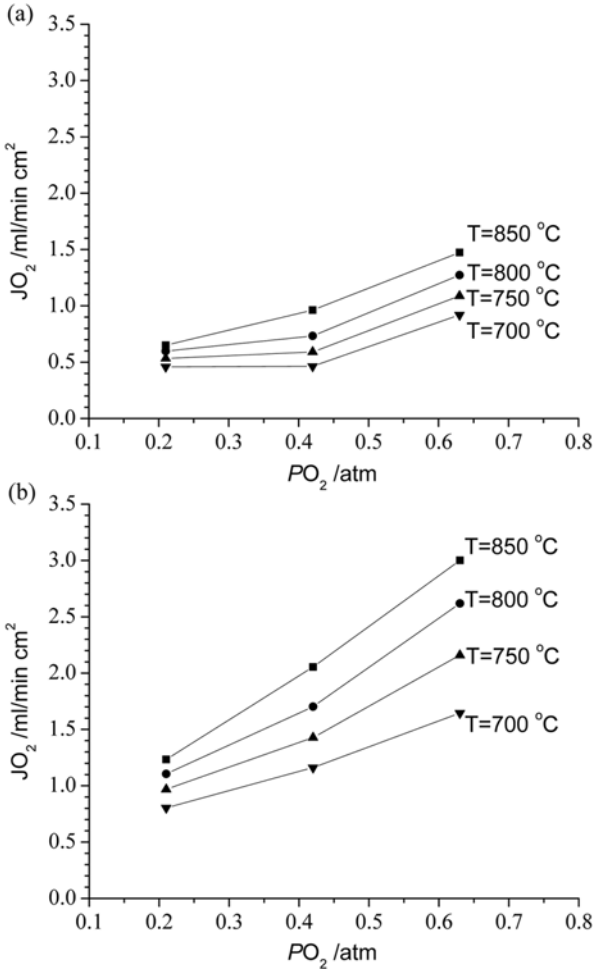

Fig. 5. Oxygen permeation flux of (a) BSCF membrane and (b) BSCF-modified BSCF membrane (tested membrane thickness: 1.0 mm) according to temperature (700-850 °C) and oxygen partial pressure (0.21, 0.42 and 0.63 atm). Lines were connected for visual guidance.

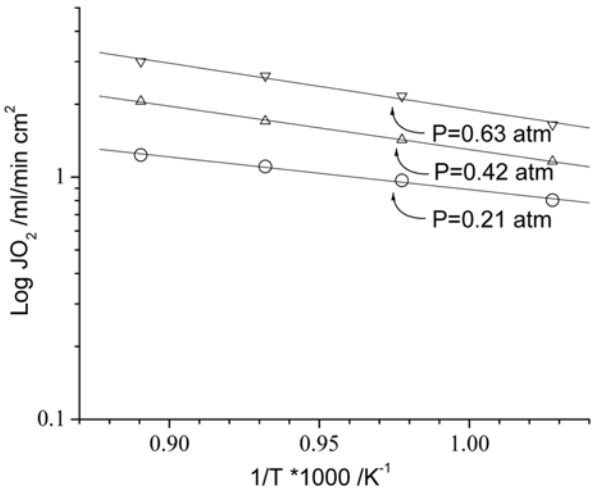

Fig. 6. Arrhenius plot of ln JO_2 of BSCF-modified BSCF membrane (tested membrane thickness: 1.0 mm) as a function of 1/T for three different oxygen pressures.

850 °C. In conclusion, the surface morphology of the BSCF membrane can affect oxygen permeation flux if the permeation process is limited also by surface exchange kinetics under mixed-control conditions, which the overall oxygen permeation flux is determined by the oxygen diffusion though the bulk and oxygen molecular-ionic exchange reaction at surfaces of the BSCF membrane.

In the range of temperature considered in this work, Arrhenius-type relations for the BSCF-modified BSCF membrane were qualitatively evaluated under different oxygen partial pressure. As shown in Fig. 6, the calculated oxygen permeation fluxes, represented by the solid curves, are again in reasonable agreement with the measurement data (markers) and all the data fit well with the Arrhenius-type dependence on the temperature. The oxygen permeation fluxes of the BSCF-modified BSCF membrane increased with the oxygen partial pressure at certain temperature. The increase of the oxygen permeation flux with temperature, a thermally activated process according to Arrhenius's law, is due to higher mobility and concentration of ionic carriers in the BSCF materials [6,16,18,23]. At 700 °C and atmospheric pressure, the oxygen permeation flux of the BSCF-modified BSCF membrane is ~0.8 ml/cm^2·min, which is about 1/3 of the value achieved at relatively high oxygen partial pressure (Po_2=0.63 atm) and temperature (850 °C). The results are in good agreement with recent experiments by Lu et al. in dense $Ba_{0.5}Sr_{0.5}Co_{0.8}Fe_{02}O_{3-\delta}$ membrane disks at different pressure [23].

It is known that carbon dioxide gas can adsorb on the active site (*i.e.*, surface oxygen vacancy, cluster, defects, *etc.*) of the membrane [25]. To clarify this point, the oxygen permeability was also measured as a function of temperature (850, 800, 750 and 700 °C) for a stepwise exposure to different oxygen partial pressure (0.21 and 0.63 atm) in the absence and in the presence of carbon dioxide (300 and 500 ppm). Fig. 7 depicts the effects of carbon dioxide concentration in feed gas, pressure and temperature on oxygen permeation fluxes through BSCF-modified BSCF membranes. As shown in Fig. 7, the oxygen permeation fluxes increased with the increase of operation temperatures and oxygen partial pressure. Oxygen permeation flux of ~1.5 ml/cm^2·min at 850 °C was obtained at high oxygen partial pressure (0.63 atm) in the presence of carbon diox-

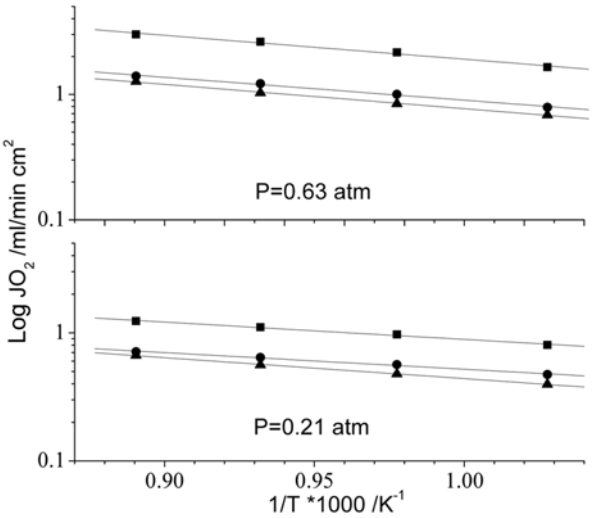

Fig. 7. Arrhenius plot of ln JO_2 of BSCF-modified BSCF membrane (membrane thickness=1.0 mm) as a function of 1/T for two different oxygen partial pressure (0.63 and 0.21 atm) with carbon dioxide. The data cover the temperature range from 850 to 700 °C (■ carbon dioxide=0 ppm, ● carbon dioxide=300 ppm, ▲ carbon dioxide=500 ppm).

ide. Moreover, we note that the apparent activation energy (slope of the line on Fig. 7) to oxygen permeation flux did not change with pressure and concentration of carbon dioxide in the gas mixture.

In general, the Arrhenius plot should be a series of parallel straight lines over the whole range of conditions if the strain-rates are controlled by a unique thermally activated process. In this case, the apparent activation energy of the overall process is equal to the activation energy of a single controlling process. From Fig. 7, it is known that Arrhenius plots for oxygen permeation fluxes consisted of a series of parallel lines. It indicated that values of pressure and/or carbon dioxide concentration did not affect the activation energy of overall process. From these results, it is confirmed that oxygen permeation through modified BSCF membrane occurred by a single-step mechanism irrespective of carbon dioxide conditions.

In order to understand the BSCF membrane stability, we have studied both pristine BSCF and BSCF-modified BSCF membrane surfaces by SEM immediately after the oxygen permeation test. Fig. 8 shows the surface and cross-sectional SEM photographs of typical BSCF membrane texture after permeation test. The visual inspection of the SEM images reported in Fig. 8(a) clearly indicates the difference between fresh membrane (*cf.* inset of Fig. 2) and BSCF membrane after oxygen permeation measurement. In instance, the surface of feed side for the BSCF membrane without any surface modification is different from the fresh BSCF membrane, and it seems that there are some materials decomposed on the surface near the grain boundary structure. Fig. 8(b) shows that the morphology of permeate-side of BSCF membrane is quite homogeneous across the surface and quite uniform surface texture in comparison with as-prepared BSCF surface (*cf.*, Fig. 2). Additionally, Fig. 8(c) shows that the BSCF morphology is homogeneous across the fractured cross section. A closer examination of the cross section reported in Fig. 8(c) for the BSCF membrane reveals that there are not many pores in the bulk membrane, indicating that the sintering temperature (1,100 °C) was sufficiently high to obtain a dense BSCF membrane.

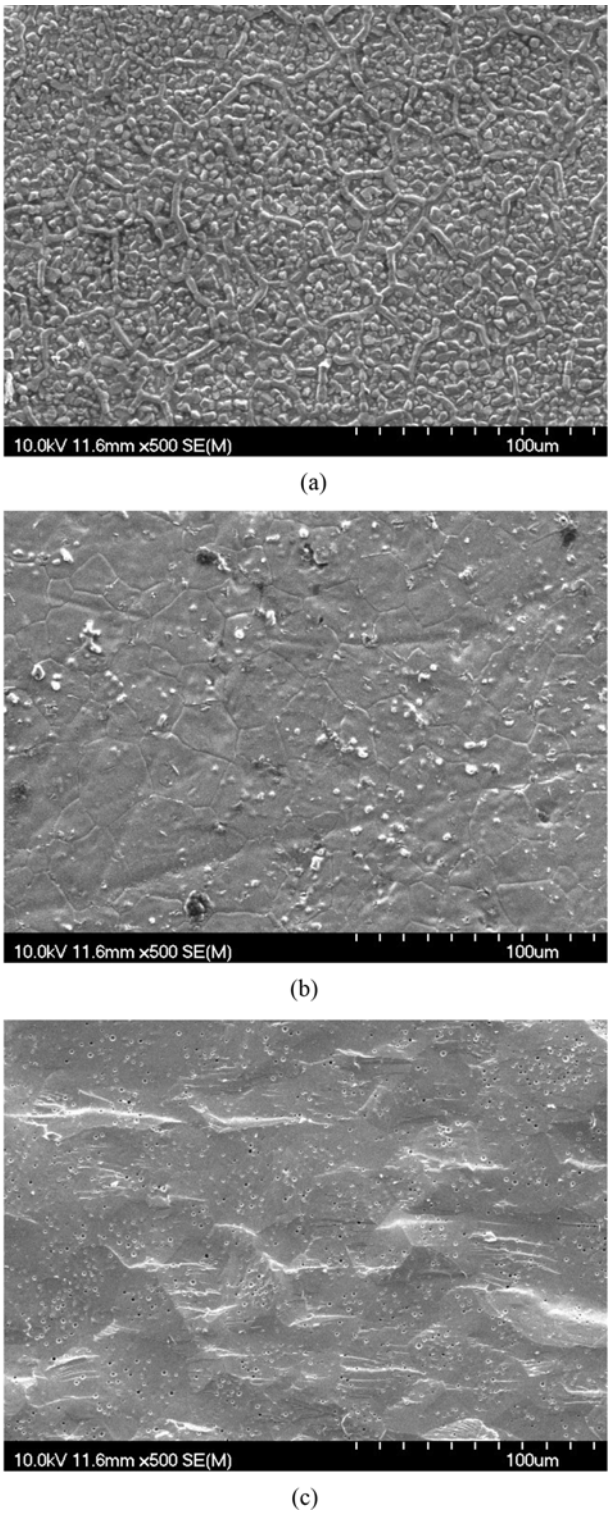

Fig. 8. SEM images of BSCF membrane without modification after permeation test; (a) feed-side, (b) permeate-side and (c) fractured cross section.

Fig. 9 shows the SEM images of BSCF-modified BSCF membrane; (a) feed-side, (b) permeate-side and (e) fractured cross sections after oxygen permeation test. It is obvious that the SEM image

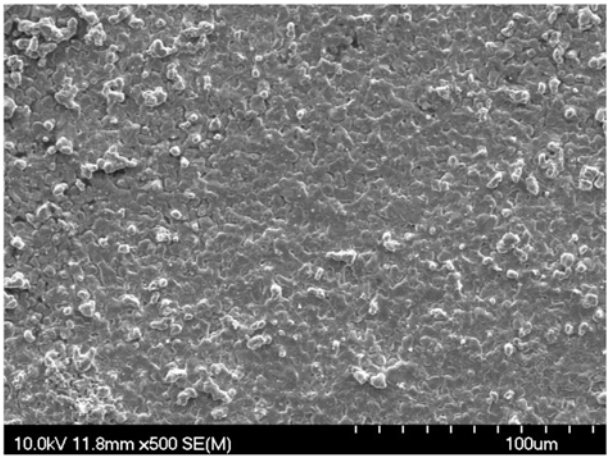

(a)

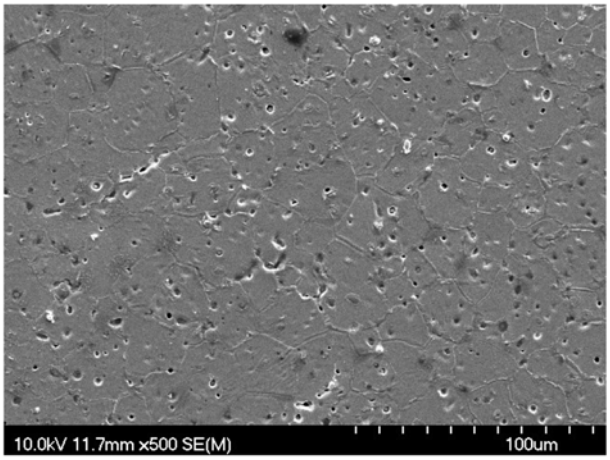

(b)

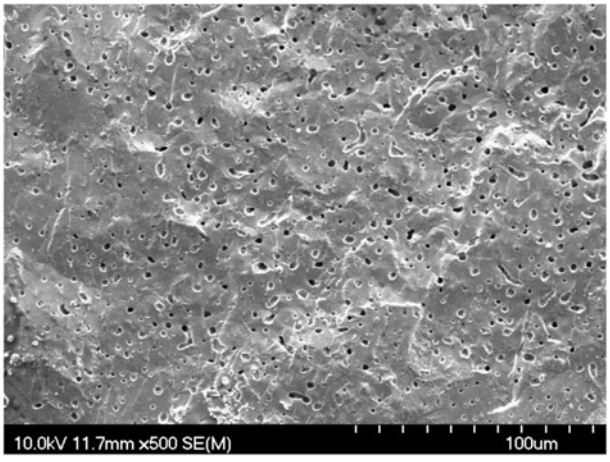

(c)

Fig. 9. SEM images of BSCF membrane with modification after permeation test; (a) feed-side, (b) permeate-side and (c) fractured cross section.

of feed side with surface modification after permeation test (Fig. 9(a)) was similar to that of feed side before permeation test (Fig. 3(d)). In fact, a large effect of carbon dioxide on the BSCF morphology can be interpreted by a formation of the carbonates on the BSCF membrane surface [10,25-27]. Nomura et al. studied the micro-

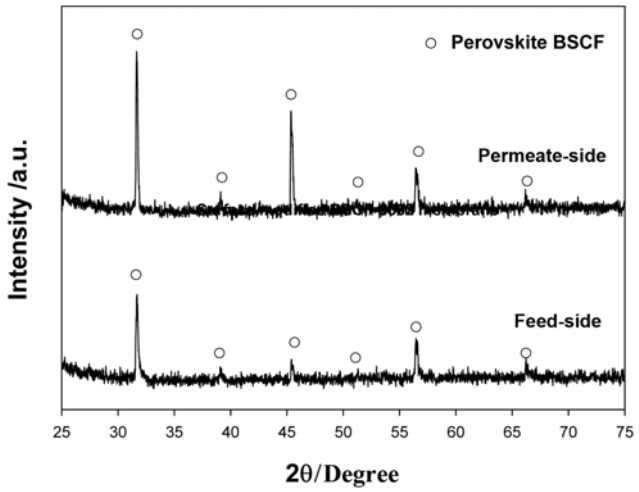

Fig. 10. XRD patterns of BSCF membrane with surface modification after permeation test.

structural change of perovskite-type oxides during their reactions with carbon dioxide, and found that dense structure makes it difficult for carbon dioxide to diffuse into the particle [28]. Yang and Lin reported an experimental and modeling study of the kinetics of carbon dioxide sorption on $La_{0.1}Sr_{0.9}Co_{0.5}Fe_{0.5}O_{3-\delta}$ at 700-900 °C [29]. In particular, the authors found that the kinetics of carbon dioxide sorption on $La_{0.1}Sr_{0.9}Co_{0.5}Fe_{0.5}O_{3-\delta}$ depends on the microstructure of the $La_{0.1}Sr_{0.9}Co_{0.5}Fe_{0.5}O_{3-\delta}$ particle and two different kinetics mechanisms were proposed for the materials with a dense and porous structure, respectively. The perovskite-type oxide solid solutions with a porous structure generally exhibit a much faster carbon dioxide sorption rate than those with a dense structure, and for the dense perovskite-type oxide samples, the carbon dioxide sorption is accompanied with oxygen desorption [28]. However, in our experiment on the basis of SEM results there is no evidence about the sorption of carbon dioxide or carbonate formation due to reaction between metal and carbon dioxide. This result also agrees with the XRD result of same membrane after permeation test (Fig. 10).

The SEM image of the permeate side of BSCF-modified BSCF membrane obtained after gas permeation test is shown in Fig. 9(b). It is also obvious that the grain boundaries of the permeate side can be easily observed though small hole was detected. The grain size and morphology in Fig. 9(b) was almost same on comparison with those of permeation side without modification (Fig. 8(b)) because BSCF modification was conducted on one side of the dense membrane.

Fig. 10 shows the XRD results for feed side and permeation side of BSCF-modified BSCF membrane after permeation test. As shown in Fig. 10, no additional peak such as carbonate or another impurity was detected in both sides of BSCF-modified membrane even though feed gas contained carbon dioxide. Especially, it notes that the membrane with surface modification was more stable in the presence of carbon dioxide like ambient air condition.

CONCLUSION

In the present study, the oxygen permeation properties of BSCF-

modified BSCF membranes was investigated as a function of temperature (850, 800, 750 and 700 °C), BSCF membrane thickness (1.0 mm and 1.6 mm) and oxygen partial pressure (0.21, 0.42 and 0.63 atm) in the absence and in the presence of carbon dioxide (300 and 500 ppm). Here the oxygen permeability of BSCF membranes without any surface modification was studied experimentally for comparison. The oxygen permeation flux of the BSCF membrane and BSCF-modified BSCF membrane increased with temperatures and oxygen partial pressures. The BSCF-modified BSCF membrane exhibited higher oxygen permeation flux than that of the BSCF membrane. The maximum oxygen permeation flux measured for BSCF-modified BSCF membrane was ~3.0 ml/cm^2·min at 850 °C exposed to oxygen partial pressure of 0.63 atm. The surface morphology is an important factor to obtain higher oxygen permeation flux and stability in the presence of carbon dioxide under mixed-control conditions.

ACKNOWLEDGEMENT

This Research was supported by a grant (16-2008-04-001-00) from Carbon Dioxide Reduction Sequestration Research Center, one of the 21st Century Frontier Programs funded by the Ministry of Education, Science and Technology of Korean government.

REFERENCES

1. B. C. H. Steel, *Mater. Sci. Eng.*, *B*, **13**, 79 (1992).
2. S.-T. Hwang, *Korean J. Chem. Eng.*, **18**, 775 (2001).
3. Z. Shao, W. Yang, Y. Cong, H. Dong, J. Tong and G. Xiong, *J. Membr. Sci.*, **172**, 177 (2000).
4. H. Wang, Y. Cong and W. Yang, *J. Membr. Sci.*, **210**, 259 (2002).
5. H. Wang, R. Wang, D. T. Liang and W. Yang, *J. Membr. Sci.*, **243**, 405 (2004).
6. S. B. Adler, *Chem. Rev.*, **104**, 4791 (2004).
7. Z. Shao and S. M. Haile, *Nature*, **431**, 170 (2004).
8. E. Magnone, *J. Fuel Cell Sci. Technol.*, **7**, 064001 (2010).
9. L. Ge, W. Zhou, R. Ran, S. Liu, Z. Shao, W. Jin and N. Xu, *J. Membr. Sci.*, **306**, 318 (2007).
10. J. Sunarso, S. Baumann, J. M. Serra, W. A. Meulenberg, S. Liu, Y. S. Lin and J. C. Diniz da Costa, *J. Membr. Sci.*, **320**, 13 (2008).
11. R. Y. Moydinov, M. N. Popova and A. R. Kaul, *Doklady Chemistry*, **402**, 88 (2005).
12. H. J. M. Bouwmeester, H. Kruidhof and A. J. Burggraaf, *Solid State Ionics*, **72**, 185 (1994).
13. C. Ftikos, S. Carter and B. C. H. Steele, *J. Eur. Ceram. Soc.*, **12**, 79 (1993).
14. E. Bucher, A. Egger, P. Ried, W. Sitte and P. Holtappels, *Solid State Ionics*, **179**, 1032 (2008).
15. S. Carter, A. Selcuk, R. J. Chater, J. Kajda, J. A. Kilner and B. C. H. Steele, *Solid State Ionics*, **53-56**, 597 (1992).
16. E. Girdauskaite, H. Ullmann, V. V. Vashook, U. Guth, G. B. Caraman, E. Bucher and W. Sitte, *Solid State Ionics*, **179**, 385 (2008).
17. A. Ghadimi, M. A. Alaee, A. Behrouzifar, A. A. Asadi and T. Mohammadi, *Desalination*, DOI:10.1016/j.desal.2010.11.022 (2010).
18. W. K. Hong and G. M. Choi, *J. Membr. Sci.*, **346**, 353 (2010).
19. Z. Chen, R. Ran, Z. Shao, H. Yu, J. C. Diniz da Costa and S. Liu, *Ceram. Int.*, **35**, 2455 (2009).
20. Q. Jiang, K. J. Nordheden and S. M. Stagg-Williams, *J. Membr. Sci.*, DOI:10.1016/j.memsci.2010.11.073 (2010).
21. J. H. Park, J. P. Kim and S. H. Son, Greenhouse Gas Control Technologies 9, Proceedings of the 9th International Conference on Greenhouse Gas Control Technologies (GHGT-9), 16-20 November 2008, Washington DC, USA, *Energy Procedia*, **1**, 369 (2009).
22. E. Magnone, M. Miyayama and E. Traversa, *J. Electrochem. Soc.*, **156**, B1059 (2009).
23. H. Lu, Y. Cong and W. S. Yang, *Solid State Ionics*, **177**, 595 (2006).
24. Z. Shen, P. Lu, G. Yan and X. Hu, *Mater. Lett.*, **64**, 980 (2010).
25. P. Zeng, Z. Chen, W. Zhou, H. Gu, Z. Shao and S. Liu, *J. Membr. Sci.*, **291**, 148 (2007).
26. S. Engels, F. Beggel, M. Modigell and H. Stadler, *J. Membr. Sci.*, **359**, 93 (2010).
27. Z. Yáng, A. S. Harvey and L. J. Gauckler, *Scr. Mater.*, **61**, 1083 (2009).
28. K. Nomura, Z. Homonnay, G. Juhasz, A. Vertes, H. Donen and T. T. s. Sawada, *Hyperfine Interact.*, **139-140**, 297 (2002).
29. Q. Yang and Y. S. Lin, *Ind. Eng. Chem. Res.*, **45**, 6302 (2006).